Pseudo-Lithium Vacancies in Hydrogen Rich Li_3OCl

Supporting Information

Benjamin A. D. Williamson,[1] Kristoffer Eggestad,[1] and Sverre M. Selbach[1]

[1] *Department of Materials Science and Engineering, NTNU Norwegian University of Science and Technology, Trondheim, Norway*

1. STRUCTURAL PROPERTIES

The calculated structural parameters and atomic distances are given in Table S1.

Table S1: The structural parameters of Li_3OCl as calculated using the PBEsol and HSE06 functionals.

	spacegroup	a = b = c (Å)	$\alpha = \beta = \gamma$ (°)	$d_{Li\text{-}O}$ (Å)	$d_{Li\text{-}Li}$ (Å)	$d_{Li\text{-}X}$ (Å)
HSE06	$Pm\bar{3}m$	3.85	90.00	1.92	2.72	2.72
PBEsol	$Pm\bar{3}m$	3.84	90.00	1.92	2.72	2.72

2. ELECTRONIC STRUCTURE

The band structure and density of states (DOS) for Li_3OCl is given in Figures S1. The DOS at the valence band maximum (VBM) and conduction band minimum (CBM) is shown, and a detailed breakdown of the percentage of states in terms of their elements and constituent orbitals is given in Table S2.

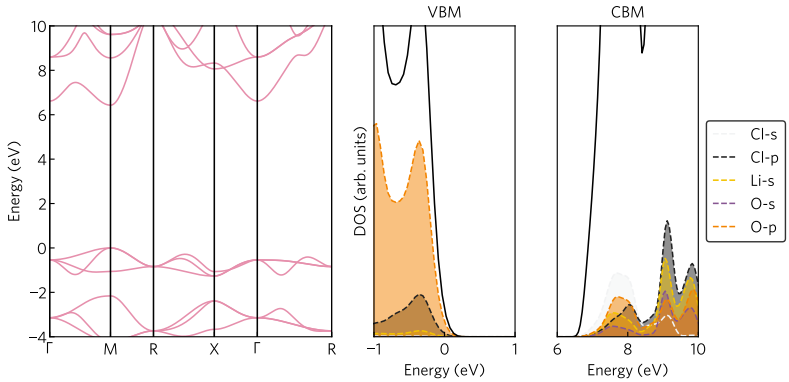

Figure S1: The electronic band structure and density of states (DOS) at the valence band maximum (VBM) and conduction band minimum (CBM) for Li_3OCl as calculated using the HSE06 functional. For the band structure and DOS the VBM is centred at 0eV.

Table S2: The percentage of states at the valence band maximum (VBM) and conduction band minimum (CBM) of Li_3OCl as calculated using the HSE06 functional.

	VBM			CBM		
	Cl	Li	O	Cl	Li	O
s	0.0	3.0	0.0	31.0	0.0	0.0
p	17.0	0.0	80.0	0.0	69.0	0.0
d	0.0	0.0	0.0	0.0	0.0	0.0

3. THERMODYNAMIC STABILITY AND DEFINING A TEMPERATURE-DEPENDENT CHEMICAL POTENTIAL SPACE

Due to the metastability of Li_3OCl a chemical stability region at 0K is not realisable due to the breakdown into constituent phases. *a priori* knowledge of the synthesis of a material can give insight into kinetically stabilised phases, such that calculation of the chemical potential stability region may be approximated through kinetic stabilisation towards one or more components on the phase diagram[1]. In terms of a wholly structure agnostic procedure to calculate the stability region, temperature dependence of the limiting phases of Li_3OCl must be calculated. In this study, the quasi harmonic approximation (QHA) is used in order to gain free energies from volume expansion and phonon calculations for each of the solid phases (Li_3OCl, $LiClO_4$, Li_2O, LiH, LiOH, LiCl). For the gas phases, (O_2, Cl_2, H_2, H_2O, H_2O_2, HCl), a straight forward gas phase approximation is used.

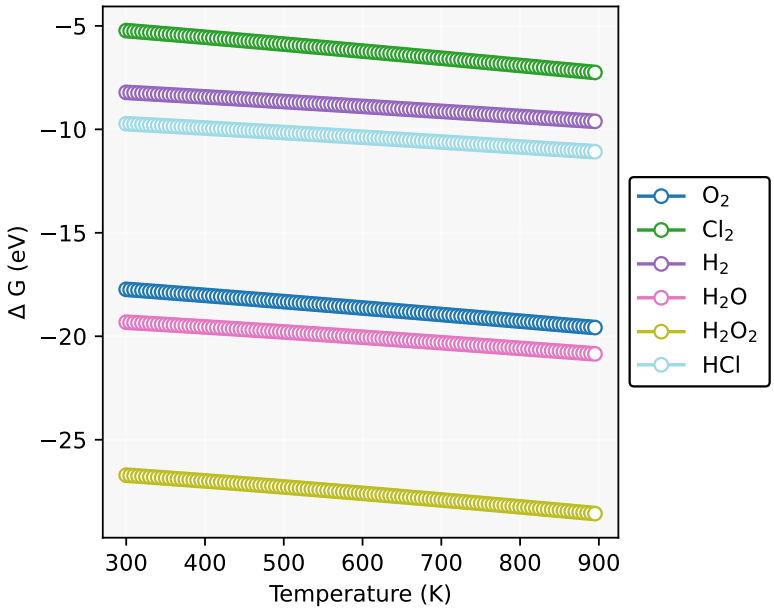

Figure S2: The Gibbs free energy of the gaseous species related to the limits of H-doped Li_3OCl using the PBEsol functional

Table S3: The calculation parameters and calculated total energy (per formula unit) for all the solid limiting phases using the HSE06 and PBEsol functionals.

Compound	Space group	k-point mesh	HSE06 (eV)	PBEsol (eV)
Li_3OCl	$Pm\bar{3}m$	$5 \times 5 \times 5$	-25.071	-22.328
Li_2O	$Fm\bar{3}m$	$9 \times 9 \times 9$	-18.030	-13.959
$LiCl_a$	$Fm\bar{3}m$	$8 \times 8 \times 8$	-10.169	-6.904
$LiCl_b$	$P6_3mc$	$7 \times 7 \times 4$	-20.409	-13.734
$LiClO_4$	$Pnma$	$2 \times 2 \times 2$	-44.0167	-25.436
LiH	$Fm\bar{3}m$	$9 \times 9 \times 9$	-6.663	-5.996
LiOH	$P4/nmm$	$7 \times 7 \times 5$	-19.117	-14.428

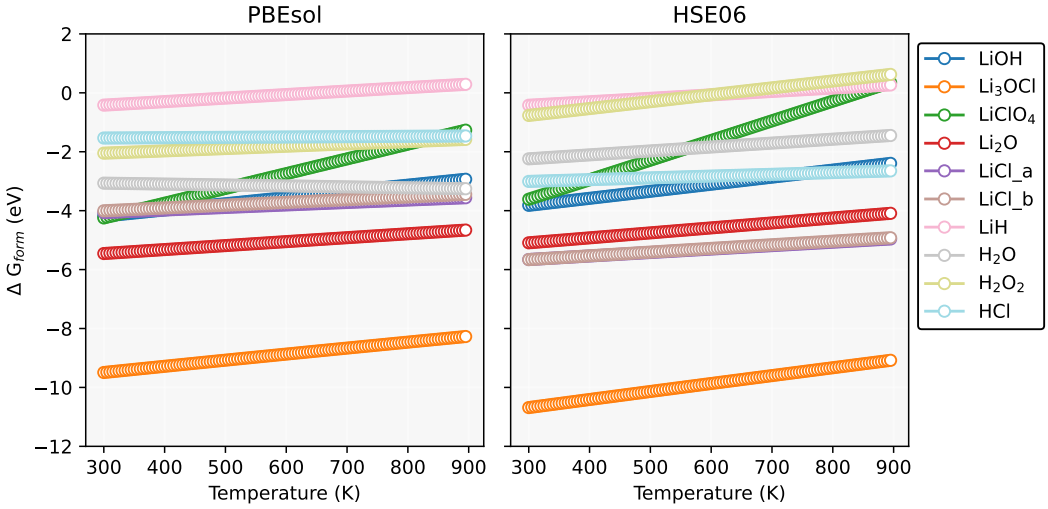

Figure S3: The Gibbs Free energies of formation as a function of temperature for each condensed phase limiting phase as calculated using the QHA approximation and the PBEsol functional.

4. CHEMICAL POTENTIAL STABILITY REGION

Table S4: The chemical potential limits as calculated using the HSE06 functional within the QHA approximation at 750K. The chemical potential for hydrogen (μ_H) is included for reference for the doped species.

	μ_{Li}	μ_O	μ_{Cl}	(μ_H)
0	0.000000	-4.349200	-5.141400	0
1	-2.174600	0.000000	-2.966800	-0.826699

[H]

5. DETERMINATION OF THE "EXPERIMENTALLY ACCESSIBLE" OXYGEN CHEMICAL POTENTIAL REGION

The experimentally accessible μ_O region can be determined using the equation outlined by Reuter and Scheffler[2]:

$$\mu_O(T,p^0) = \frac{1}{2}[H(T,p^0,O_2) - H(0K,p^0,O_2)] - \frac{1}{2}T[S(T,p^0,O_2) - S(0K,p^0,O_2)] \quad (1)$$

where T, H, and S are temperature, enthalpy, and entropy, respectively. $p^0 = 1$atm (with reference to a zero state; $\mu_O(0K,p^0) = \frac{1}{2}E_{O_2}^{\text{total}} = 0$).[3,4].

6. GIBBS FREE ENERGY OF REACTION FOR SYNTHETIC ROUTES OF LI$_3$OCL

The synthetic routes for various synthesis methods as outlined in refs [5, 6] are given in equations 2-5 and corresponding Gibbs free energy of reaction (ΔG_{react}) as a function of temperature, calculated with HSE06, is presented in Figure S4. For Reactions 3-5 LiOH and LiH is present in the synthesis route, leading to the speculation that OH or H is present within the Li_3OCl lattice, or is indeed fully formed Li_2OHCl or other hydroxide analogues.[6] Reaction 2 is the only synthetic route where Li_3OCl is kinetically stabilised by LiCl and Li_2O and does not include OH in any form, however the reaction is slow and gives a low yield.[5] From our calculations, Reactions 4-5 possess negative free energies indicating spontaneous formation of Li_3OCl, consistent with the ease with which Li_3OCl is formed in experiment.[5] In reaction 3, spontaneous formation only occurs after 500K (226°C), which is $\sim$ 100°C below the experimental synthesis temperature. In Reaction 2, spontaneous formation is expected at 750K, ($\sim$ 477°C) consistent with the experimental synthesis conditions of ($\sim$ 500°C). The slow formation is expected due to poor correlation of ΔG_{react} with experiment.

$$Li_2O + LiCl \xrightarrow{500\,^\circ C} Li_3OCl \quad (2)$$

$$LiCl + 2\,LiOH \xrightarrow[\text{high vacuum, several days}]{\text{330-360}\,^\circ C} Li_3OCl + H_2O \quad (3)$$

$$Li + LiOH + LiCl \xrightarrow[\text{high vacuum, 10 hrs}]{600\,^\circ C} Li_3OCl + \frac{1}{2}H_2 \quad (4)$$

$$LiH + LiOH + LiCl \xrightarrow[1\,\text{hr}]{480\,^\circ C} Li_3OCl + H_2 \quad (5)$$

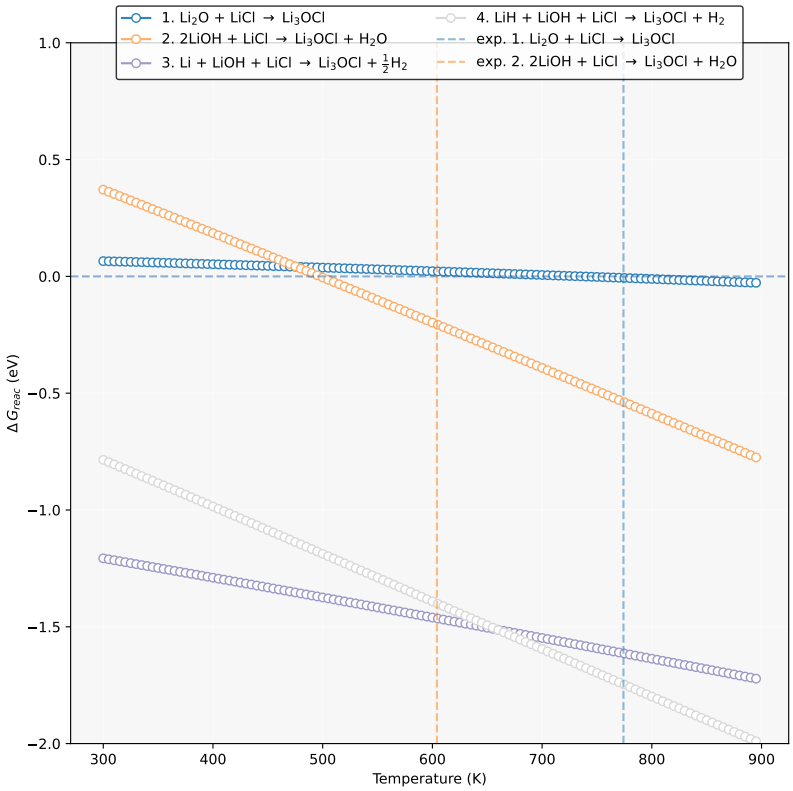

Figure S4: The Gibbs Free energy of reaction (ΔG_{reac}) for different synthetic routes given in equations 2-5 as calculated with the HSE06 functional. Experimental synthesis temperatures are given as dashed vertical lines taken from ref.[5].

7. DEFECT THERMODYNAMICS

Table S5: The tabulated total energies (E_{total}), potential energy alignment (ΔE^{pot}), image charge correction (E^{IC}_{corr}) and band filling correction (E^{BF}_{corr}) for each *intrinsic* defect species and its constituent charge state (q).

Defect	q	E_{total} (eV)	ΔE^{pot} (eV)	E^{IC}_{corr} (eV)	E^{BF}_{corr} (eV)
			Vacancies		
V_{Cl}	0	-749.046	0.000	0.000	0.000
	1	-751.156	-0.128	0.076	0.000
V_{Li}	-1	-751.610	-0.055	0.076	0.000
	0	-752.332	0.000	0.000	0.000
V_{O}	0	-743.079	0.000	0.000	0.000
	1	-747.193	-0.009	0.076	0.000
	2	-750.558	0.005	0.302	0.000
			Antisites		
Cl_O	0	-748.645	0.000	0.000	-0.068
	1	-755.114	0.113	0.076	0.000
O_{Cl}	-1	-758.797	-0.099	0.076	0.000
	0	-760.091	0.000	0.000	0.000
			Interstitials		
Cl_i	-1	-757.587	0.077	0.076	0.000
	0	-759.070	0.000	0.000	0.000
Li_i	0	-756.333	0.000	0.000	-0.130
	1	-762.816	0.029	0.076	0.000
	-2	-759.700	-0.037	0.302	0.000
O_i	-1	-763.173	0.014	0.076	0.000
	0	-764.469	0.000	0.000	0.000

Table S6: The tabulated total energies (E_{total}), potential energy alignment (ΔE^{pot}), image charge correction (E^{IC}_{corr}) and band filling correction (E^{BF}_{corr}) for each *extrinsic* species and its constituent charge state (q).

Defect	q	E_{total} (eV)	ΔE^{pot} (eV)	E^{IC}_{corr} (eV)	E^{BF}_{corr} (eV)
			H-doping		
H_{Cl}	0	-754.294	0.000	0.000	0.000
	-1	-742.062	-0.052	0.076	0.000
H_O	0	-746.508	0.000	0.000	0.000
	1	-752.659	0.002	0.076	0.000
	-1	-756.312	-0.035	0.076	0.000
H_i	0	-759.315	0.000	0.000	0.000
	1	-764.746	0.046	0.076	0.000
			H-doping clusters		
	-1	-754.113	-0.112	0.076	0.000
HH_{Cl}	0	-756.564	0.000	0.000	0.000
	1	-760.982	-0.077	0.076	0.000
HO_{Cl}	0	-766.535	0.000	0.000	0.000
	-1	-745.248	-0.041	0.076	-0.086
HH_O	0	-751.624	0.000	0.000	0.000
	1	-754.063	0.011	0.076	0.000
	2	-757.839	0.030	0.302	0.000
	-2	-747.701	0.090	0.302	-0.086
HCl_O	-1	-747.701	0.090	0.076	-0.086
	0	-754.251	0.000	0.000	0.000
	1	-756.228	0.123	0.076	0.000
HH_i	0	-764.405	0.000	0.000	0.000
HO_i	-1	-767.730	0.001	0.076	0.000
	0	-769.278	0.000	0.000	0.000
HCl_i	0	-762.342	0.000	0.000	0.000

8. PARTIAL CHARGE DENSITIES FOR V_{Li}, V_O, AND Li_i

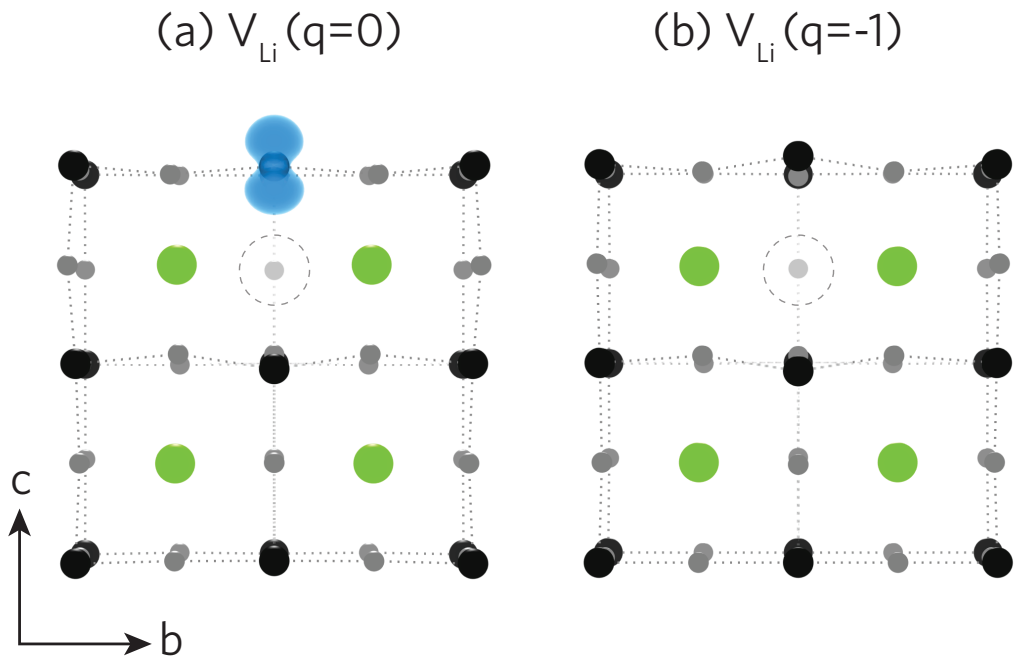

Figure S5: The partial charge densities for V_{Li} (dashed circle) in the q=0 (a) and q=-1 (b) charge states. The electron hole (blue) induced by V_{Li} is localised on an adjacent O 2p orbital. The colours correspond thus: Li = grey, O = black, Cl = green. The partial charge density is plotted from 0-0.02 $Å^{-1}$.

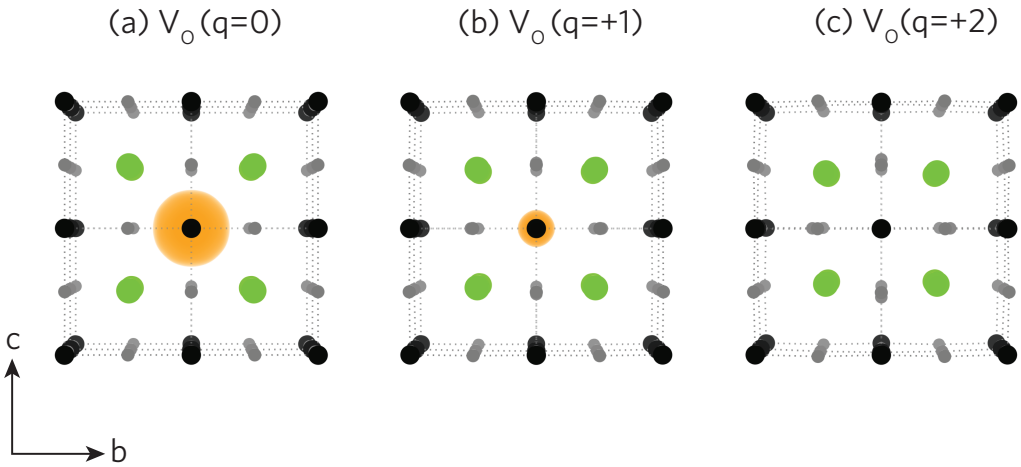

Figure S6: The partial charge densities for V_O in the q=0 (a) and q=+1 (b), and q=+2 (c) charge states. The electron(s) (orange) induced by V_O is localised within the vacancy site. The colours correspond thus: Li = grey, O = black, Cl = green. The partial charge density is plotted from 0-0.01 $Å^{-1}$.

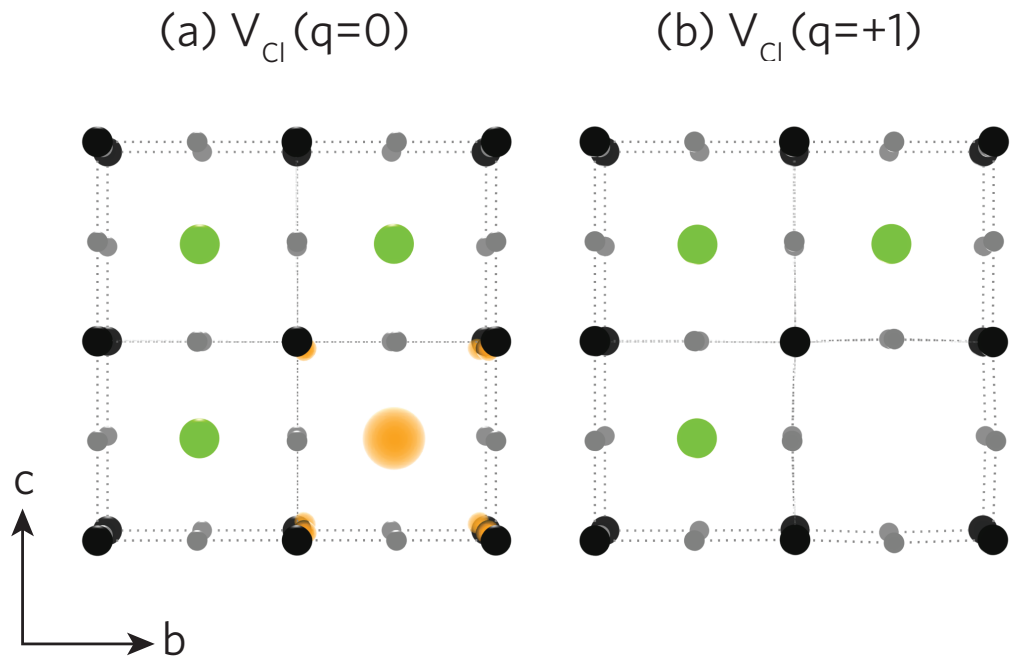

Figure S7: The partial charge densities for V_{Cl} in the q=0 (a) and q=+1 (b) charge states. The electron (orange) induced by V_{Cl} is localised within the vacancy site. The colours correspond thus: Li = grey, O = black, Cl = green. The partial charge density is plotted from 0-0.01 $Å^{-1}$.

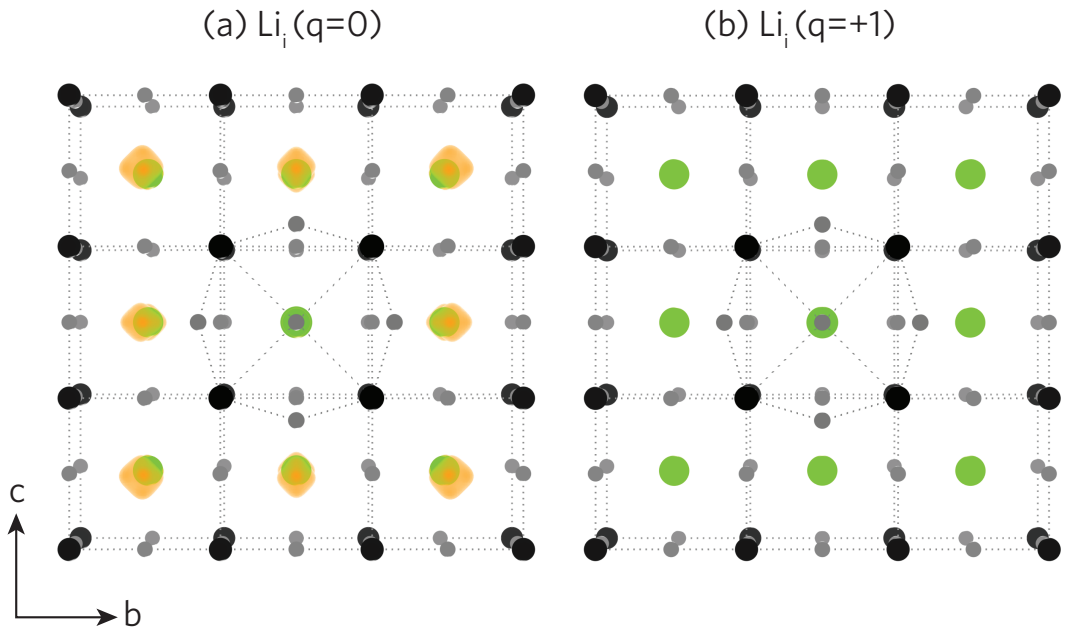

Figure S8: The partial charge densities for Li_i in the q=0 (a) and q=+1 (b) charge states. The electron (orange) induced by Li_i is delocalised across Cl s orbitals at the conduction band minimum. The colours correspond thus: Li = grey, O = black, Cl = green. The partial charge density is plotted from 0-0.0015 $Å^{-1}$. The cell has been shifted so that Li_i is centred.

[1] A. G. Squires, J. M. Dean, and B. J. Morgan, Chemrxiv **0.26434/chemrxiv-2021-hzrls** (2021).

[2] K. Reuter and M. Scheffler, Phys. Rev. B **65**, 035406 (2001).

[3] F. H. Taylor, J. Buckeridge, and C. R. A. Catlow, Chem. Mater. **28**, 8210 (2016).

[4] J. E. N. Swallow, B. A. D. Williamson, T. J. Whittles, M. Birkett, T. J. Featherstone, N. Peng, A. Abbott, M. Farnworth, K. J. Cheetham, P. Warren, D. O. Scanlon, V. R. Dhanak, and T. D. Veal, Advanced Functional Materials **28**, 1701900 (2018).

[5] S. Li, J. Zhu, Y. Wang, J. W. Howard, X. Lu, Y. Li, R. S. Kumar, L. Wang, L. L. Daemen, and Y. Zhao, Solid State Ionics **284**, 14 (2016).

[6] I. Hanghofer, G. J. Redhammer, S. Rohde, I. Hanzu, A. Senyshyn, H. M. R. Wilkening, and D. Rettenwander, Chem. Mater. **30**, 8134 (2018).